ROYAL SOCIETY
OF CHEMISTRY

PAPER

Check for updates

Design of polyurethane composite foam obtained from industrial PET wastes and MXenes for EMI shielding applications†

Edina Rusen, [ID] ‡*[a] Alexandra Mocanu, [ID] ‡[ab] Gabriela Toader,‡[c] Aurel Diacon, [ID] [c] Cosmin Romanitan,[b] Ovidiu Iorga,[d] Martino Aldrigo, [ID] [b] Catalin Parvulescu,[b] Raul Mitran [ID] [e] and Oana Brincoveanu[bf]

The primary aim of this study was to synthesize and characterize polyurethane (PUR) foams derived from the depolymerization products of poly(ethylene terephthalate) (PET) and MXenes (Nb$_2$AlC). The depolymerized PET products were produced through a zinc acetate-catalyzed glycolysis process using diethylene glycol (DEG) as solvent. These glycolysis products were then reacted with 4,4′-diphenylmethane diisocyanate (MDI), commercial polyols, and MXenes to produce the PUR foams. The resulting materials were characterized using FT-IR, SEM, EDX mapping, mechanical testing, thermal analysis, and electromagnetic interference (EMI) shielding assessments. The analysis revealed that specimens with a higher concentration of the filler (3.55%) exhibited superior mechanical properties, while the thermal behavior remained relatively unchanged. The sample containing 2.56% of MXenes showed significant potential as an effective EMI shielding material in the 8–9 GHz frequency range, while the blank sample provided the best performance between 9–13 GHz, mostly due to a bigger high-frequency absorption in the upper part of the X band. Regarding mechanical performance, the compression force increased slightly from 1013.31 N to 1013.71 N as the Mxenes concentration increased from 2.56% to 3.55%.

1 Introduction

Polyethylene terephthalate (PET) is a highly significant and widely utilized engineering thermoplastic, commonly found in products like water bottles, food packaging, and synthetic textiles.[1] Its lightweight, durability, and versatility make PET an indispensable material in modern-day society.[2]

The increasing use of PET has led to a global crisis in waste management, as the improper disposal of PET products has caused significant environmental damage.[3] Recycling PET is essential for addressing this issue, as it can greatly decrease the amount of plastic waste that ends up in landfills or oceans. The recycling process involves collecting used PET products, processing them into new materials, and repurposing them for the production of new products.

The recycling strategy defines 4 different categories for PET waste: re-extrusion (primary recovery), mechanical recycling (secondary recycling), chemical recycling (tertiary recycling), and energy recovery (quaternary recycling).[4]

Chemical recycling is a key strategy that allows PET waste to gain new functionalities through closed-loop, upcycling, or downcycling methods.[5] For example, closed-loop recycling converts PET waste into products with comparable functionality, reducing the demand for virgin monomers. Upcycling, on the other hand, enhances the value of PET-based products by transforming PET bottle waste into high-performance textiles or mechanically resilient composites.[6,7] Lastly, downcycling converts PET into lower-value or lower-quality products, such as construction materials or non-food packaging which are harder to recycle although their lifespan is extended.[7]

Thus, based on these chemical directions, a good opportunity to give PET waste a new life determined many researchers to develop new chemical recycling methods that involve mainly: (i) hydrolysis method; (ii) methanol alcoholysis method; (iii)

[a]Faculty of Chemical Engineering and Biotechnologies, National University of Science and Technology Politehnica Bucharest, 1-7 Gh. Polizu Street, Bucharest, 011061, Romania. E-mail: edina_rusen@yahoo.com

[b]National Institute for Research and Development in Microtechnologies—IMT Bucharest, 126A Erou Iancu Nicolae Street, 077190 Bucharest, Romania

[c]Military Technical Academy, "Ferdinand I", 39-49 G. Cosbuc Blvd., Bucharest, 050141, Romania

[d]Research and Innovation Center for CBRN Defense and Ecology, 225 Oltenitei Avenue, District 4, Bucharest, Romania

[e]"Ilie Murgulescu" Institute of Physical Chemistry, Romanian Academy, 202 Splaiul Indepedentei, Bucharest, 060021, Romania

[f]Research Institute of the University of Bucharest, ICUB Bucharest, Soseaua Panduri, nr. 90, Sector 5, Bucharest, 050663, Romania

† Electronic supplementary information (ESI) available. See DOI: https://doi.org/10.1039/d4ra07447e

‡ Co-authors equally contributed to this study.

ethylene glycol alcoholysis method; (iv) alcohol–alkali combined depolymerization method, and (v) ammonolysis.[8]

Our team was involved in PET recycling by the chemical method through glycolysis reactions both in conventional[9] and microwave-assisted reactions.[10] To produce new innovative composite materials our research was continuously directed to the reuse of oligomers, respectively monomers resulting from the depolymerization process of PET. Thus, the first innovative products that we obtained were polyurethane adhesives and rigid polyurethane foams.[11]

More recently, our team investigated the utilization of recycled PET by the chemical method to synthesize a new type of polyurethane flexible foam used as a filling agent namely fly ash, and glass wastes,[12] respectively red mud and pyrite.[13]

In both articles previously published, the mechanical properties of the polyurethane flexible foams decreased as the amount of the filling agent increased. This behavior is attributed to the micro- to millimeter-scale size of the filling agent, which leads to non-homogeneous foam synthesis. Reducing the size of the filling agent could potentially improve uniformity, enhance mechanical properties, and ensure reproducibility of the formulated specimens, but this would likely result in higher production costs. To justify these increased costs, the new foams must demonstrate significantly superior properties compared to those currently available on the market.

MXenes is the denomination of several transition metal carbides, nitrides, or carbonitrides typically obtained by chemical delamination of 3D ternary (or quaternary) compounds known as MAX phases.[14] MXenes have a general formula $M_{n+1}X_nT_x$ (n = 1–3), where M represents a transition metal (such as Sc, Ti, Zr, Nb, and others), X is carbon and/or nitrogen and T_x represents the hydroxyl, oxygen, or fluorine terminations derived from the synthesis procedures.[15] Since their discovery of $Ti_3C_2T_x$ – 2D compound in 2011,[16] nearly thirty compounds have already been synthesized and many more were predicted theoretically.

Today, with the rapid advancement of electronic technology and digital communication systems, particularly in fifth-generation (5G) communication, electromagnetic (EM) radiation has emerged as a new form of environmental pollution.[17] The heavy EM radiation contamination not only severely disrupts the functioning of electronic equipment but also harms mankind's health and compromises information security.[18] Although traditional metallic materials, owing to their superior electrical conductivity, have been extensively applied as outstanding EMI shielding materials, their shortcomings of poor mechanical flexibility, exceptionally high density, costly processing, and vulnerability to corrosion significantly prevent their application.[19] As new materials for EMI shielding are evolving, polyurethane foams have been regarded as potential alternatives because of their lightweight, easy processing, low cost, and excellent anticorrosive properties compared to metal-based materials.[20,21] Additionally, MXenes started to be intensively used in EMI shielding applications due to their superior properties in terms of electroconductivity, chemical functionality, ease of surface modification, excellent flexibility, and

facile processing in polymer matrix compared to other carbonaceous fillers like carbon nanotubes or graphene.[20,22–24]

Building on our previous work with MXenes,[25] which focused on synthesizing and characterizing nanocomposites based on polymer colloids (PC) and MXenes for EMI shielding applications – specifically in paints – this study aims to combine the properties of MXenes with polyurethane foams to create a novel material for EMI shielding. A key advantage of this new material is its low production cost, achieved by utilizing PET waste, which aligns with recycling principles and leads to the development of materials with promising mechanical, thermal, and EMI shielding properties.

2 Materials and methods

2.1 Materials

Polyethylene terephthalate (PET) having a molecular weight Mn = 25 000 g mol^{-1} was used as flakes from post-consumer bottles. Diethylene glycol (DEG) (Fluka), zinc acetate (Fluka), 4,4′-diphenylmethane diisocyanate (MDI) (Aldrich), PETOL 110 (Mn = 110 g mol^{-1}-diol) (Oltchim, S.A. Romania), PETOL 56 (Mn = 56 g mol^{-1}-triol) (Oltchim, S.A. Romania), Nb_2AlC-MXenes (Sigma-Aldrich), and triethylamine (TEA) (Aldrich) were used as received.

2.2 Methods

2.2.1 Depolymerization – glycolysis of PET.
The reaction was carried out using a reactor equipped with a mechanical stirrer, condenser, timer, and thermostat. The experiments involved 240 g of PET, 150 g of DEG, and 1.5 g of zinc acetate as catalyst. The reaction was performed under a nitrogen atmosphere at a temperature of 220 °C under continuous stirring for 2 h.

2.2.2 Synthesis of polyurethane foams.
Component **A** was obtained by mixing the PET glycolysis product with PETOL 110, PETOL 56, and different concentrations of MXenes. Component **B** consisting of MDI was added to component **A** and stirred for homogenization in the presence of 0.03 mL TEA and 0.01 mL distilled water; the creaming time was 1 min, followed by the rising step. The PUR foam formulations are presented in Table 1. In Scheme 1 the synthesis strategy for obtaining PUR foam is presented.

2.3 Characterization

2.3.1 GPC analysis.
The molecular weight of depolymerized PET was determined by gel permeation chromatography (GPC) using a PL-GPC 50 Integrated GPC/SEC System (Agilent Technologies) apparatus equipped with a refractive index detector using polystyrene as standard, and THF as a solvent, at flow rate of 1 mL min^{-1}.

2.3.2 FT-IR analysis of polyurethane foams.
The FT-IR analysis was performed on a Spectrum Two FT-IR spectrometer (PerkinElmer) with a MIRacle™ Single Reflection ATR-PIKE Technologies at 4 cm^{-1} resolution, summing 16 scans in the 4000–550 cm^{-1} region.

Table 1 The samples composition

Sample codes	Polyol from PET (g)	MDI (g)	PETOL 110 (g)	PETOL 56 (g)	Mxenes (g)
Sample 0 (blank)	3	11	3	2	0
A	3	11	3	2	0.3
B	3	11	3	2	0.5
C	3	11	3	2	0.7

2.3.3 SEM analysis and EDX mapping of the polyurethane foams. The morphological and structural characterization of all PUR foams were acquired using a Nova NanoSEM 630 Scanning Electron Microscope (FEI Company, Hillsboro, OR, USA) at an acceleration voltage of 10 kV. To prove the presence and distribution of MXenes in the whole polymer matrix, an element energy dispersive spectroscopy (EDS) system (Smart Insight AMETEK) at an acceleration voltage of 10 kV was used. The pore distribution of blank PUR foams and PUR specimens filled with MXenes was extracted from SEM images by measuring around 100 individual pores. The histograms were best fitted with the Gauss function and exhibited an unimodal distribution of the pores.

2.3.4 Determination of density for PUR samples. The density of the blank PUR and PUR foam samples modified with MXenes was determined based on the *ASTM D7710-14 – Standard Test Method for Determination of Volume and Density of Rigid and Irregularity Shaped Molded Cellular Materials*. The determinations were made in triplicate and the average values, expressed in kg m^{-3} were presented in Fig. 5 as a dependence of the filler's concentration.

2.3.5 XRD analysis of the MXenes and PUR foams loaded with MXenes. X-ray diffraction (XRD) investigations were carried out using a 9 kW Rigaku Smart Lab diffractometer, equipped with a Cu Kα1 source that provides a monochromatic beam with wavelength, $\lambda = 0.1546$ nm. The measurements were recorded in 2θ mode, while the incidence angle was fixed at 0.5° (grazing-incidence mode), using a speed of 5° min^{-1}.

2.3.6 Compression tests of the polyurethane foams. The samples underwent a uniaxial compressive test on a Titan 10 dual-column Universal Testing Machine, equipped with a 10 kN load cell and TestWise™ software. *The compressive tests were performed by adapting the ASTM D1621 – Standard Test Method for Compressive Properties of Rigid Cellular Plastics.* The cylindrical specimens (5 for each PUR foam), with dimensions of approximately 12 mm in height and 10 mm in diameter, were subjected to compressive uniaxial loading at a rate of 5 mm min^{-1}.

2.3.7 TGA analysis of the polyurethane foams. Thermogravimetric analysis (TGA/DTG) was performed on NETZSCH TG 209F1 Libra equipment by heating samples of about 5 mg in the temperature range 25–700 °C with a rate of 10 °C min^{-1} under nitrogen flow.

2.3.8 DSC analysis of the polyurethane foams. The differential scanning calorimetry (DSC) analyses were performed on a NETZSCH DSC 204 F1 Phoenix instrument. Samples weighing about 10 mg were cycled 2 times (between −50–250 °C first heat and between −50–350 °C second heat) under nitrogen flow at 10 °C min^{-1} heating rate. The second heating was used for glass transition temperature (T_g) determination.

2.3.9 Evaluation of EMI shielding properties. To assess the EMI shielding properties of the samples (Sample 0, A, B, and C) we used a calibrated Vector Network Analyzer (VNA) connected to two X-band waveguide transitions, and in between the latter, we inserted the various specimens to register the S parameters at the two ports of the VNA as previously described in our
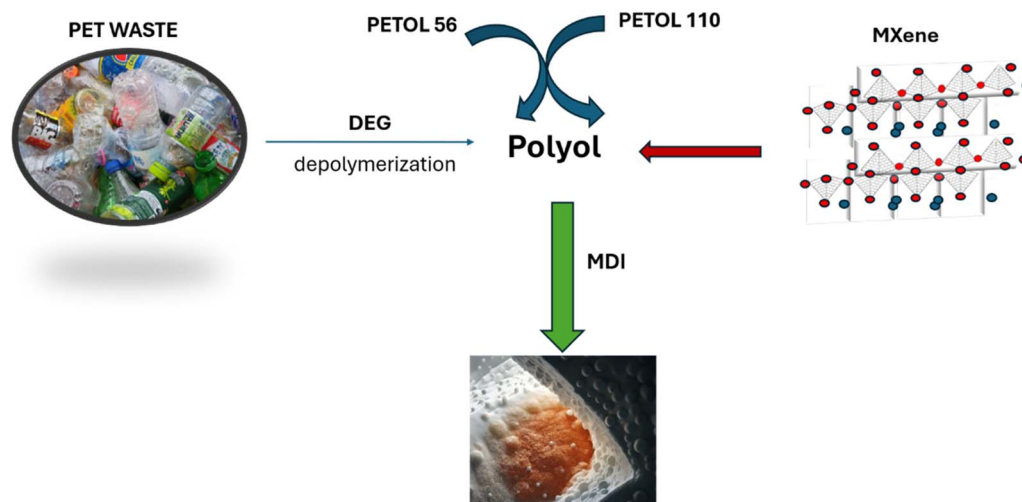
Scheme 1 The synthesis of the PUR foam filled with MXenes.

work.[25] Thus, their reflection and transmission properties were determined in a particular frequency range from 8.2 to 12.4 GHz, known as the X band.

A common method for evaluating a material's shielding properties is to calculate the total EM shielding effectiveness (SE) using eqn (1), which can be obtained from either simulations or direct measurements, when possible:[26]

$$SE \; (dB) = SE_R \; (dB) + SE_A \; (dB) \tag{1}$$

in which SE_R represents the shielding effectiveness related to the electromagnetic reflections (R), while SE_A pertains to the shielding effectiveness associated with absorption (A) phenomena. Both SE_R and SE_A can be determined using the scattering (S) parameters for a specific frequency range, specifically the reflection (S_{11} or S_{22}) and transmission (S_{21} or S_{12}) parameters of a two-port setup, described by eqn (2):[26]

$$SE \; (dB) = SE_R \; (dB) + SE_A \; (dB) = 10 \log[(1 - |S_{11}|^2)^{-1}] + 10 \log[(1 - |S_{11}|^2)/|S_{21}|^2] \tag{2}$$

Two primary physical mechanisms for modulating SE can be identified from eqn (1), respectively eqn (2): (i) EM reflections (which are enhanced in metals due to their high conductivity and minimal absorption); (ii) absorption, which is attributed to dielectric losses and low conductivity. Unlike metals, where SE cannot be adjusted, the SE of composites such as polymer-based materials can be engineered by altering the concentration of their constituents and/or fillers.

Moreover, by using eqn (3) and (4) it is also possible to extract the high-frequency conductivity σ and skin depth δ of the tested foams loaded with MXenes:[27]

$$SE_R = 35.9 + 10 \log[\sigma/(2\pi f \mu_0 \mu_r)] \tag{3}$$

$$\delta = 1 \Big/ \sqrt{\pi f \mu_0 \mu_r \sigma} \tag{4}$$

where f is the frequency, μ_0 is the vacuum permeability (equal to $4\pi \times 10^{-7}$ N A^{-2}), and μ_r is the relative permeability of the tested materials. For non-magnetic materials (like in our case study), $\mu_r = 1$.

3 Results and discussion

3.1 PET-based polyol-GPC characterization and synthesis of polyurethane foams

The first step of this study involved the depolymerization of PET flakes and the characterization of glycolysis products. The kinetics of the reaction was presented by our group elsewhere.[9] Based on the previous experience, the PET flakes from post-consumer bottles were degraded in DEG as a glycolysis agent in the presence of zinc acetate catalyst at a temperature of 220 °C for 2 hours under a nitrogen atmosphere (as detailed in Section 2.2.1). The glycolysis products were investigated by GPC analysis to determine the molecular weight (Mn) and the dispersity index (PD) of the final product. Thus, the depolymerized PET registered a Mn of 420 g mol^{-1}, while PD indicated a value of 1.2. These results are considered important for the next step

of our study which consisted in the formulation of polyurethane foams based on the Mn of the polyol resulting from the depolymerization of PET. Thus, the synthesis of the polyurethane foams involved the use of MXenes, while keeping a constant molar ratio of the NCO/OH groups as presented in Table 1. The concentration of the filling agent (MXenes) varied from 1.55 up to 3.55% (weight), the codes representing the filler concentration.

3.2 FT-IR analysis of the polyurethane foams

To evidence the reaction between the PET-based polyol and the isocyanate component, the PUR-based samples were investigated by FT-IR analysis (Fig. 1).

In Fig. 1 the FT-IR analysis evidenced the characteristic vibrations of polyurethane structure for all samples filled with MXenes. The signal from 3342 cm^{-1} attributed to NH stretching and the signal from 1716 cm^{-1} assigned to C=O stretching confirmed the formation of urethane groups due to the reaction between the OH groups and NCO groups from MDI.[28] Vibrations of CH$_2$, respectively CH$_3$ groups were registered at 2925 cm^{-1} and 2857 cm^{-1}. The NCO group from 2267 cm^{-1} was attributed to the terminal groups of the polymeric chain. The C=C registered at 1598 cm^{-1} can be assigned to the MDI hard segments' aromatic rings or those from the terephthalate unit. The peak from 1520 cm^{-1} was attributed to the N–H bending in the plane of the amide group. Another indication that the reaction took place was proved by the CN stretching vibrations in amine assigned at 1219 cm^{-1}.[29] Also, for samples A, B, and C the vibration specific for the MAX phase at 550 cm^{-1} is noticed.[30] It can be concluded that the above-mentioned samples are consistent with their chemical composition based on PUR foams and MXenes components.

3.3 SEM analysis, the pore size distribution and the density of the polyurethane foams

The next step of this study involved examining the morphology of all samples using SEM analysis. As shown in Fig. 2, the
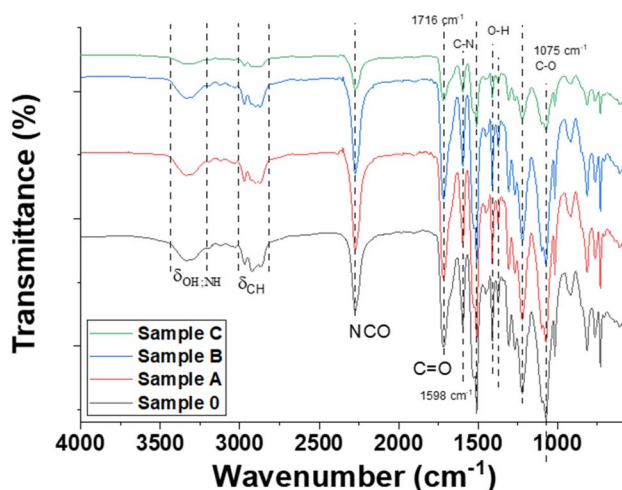

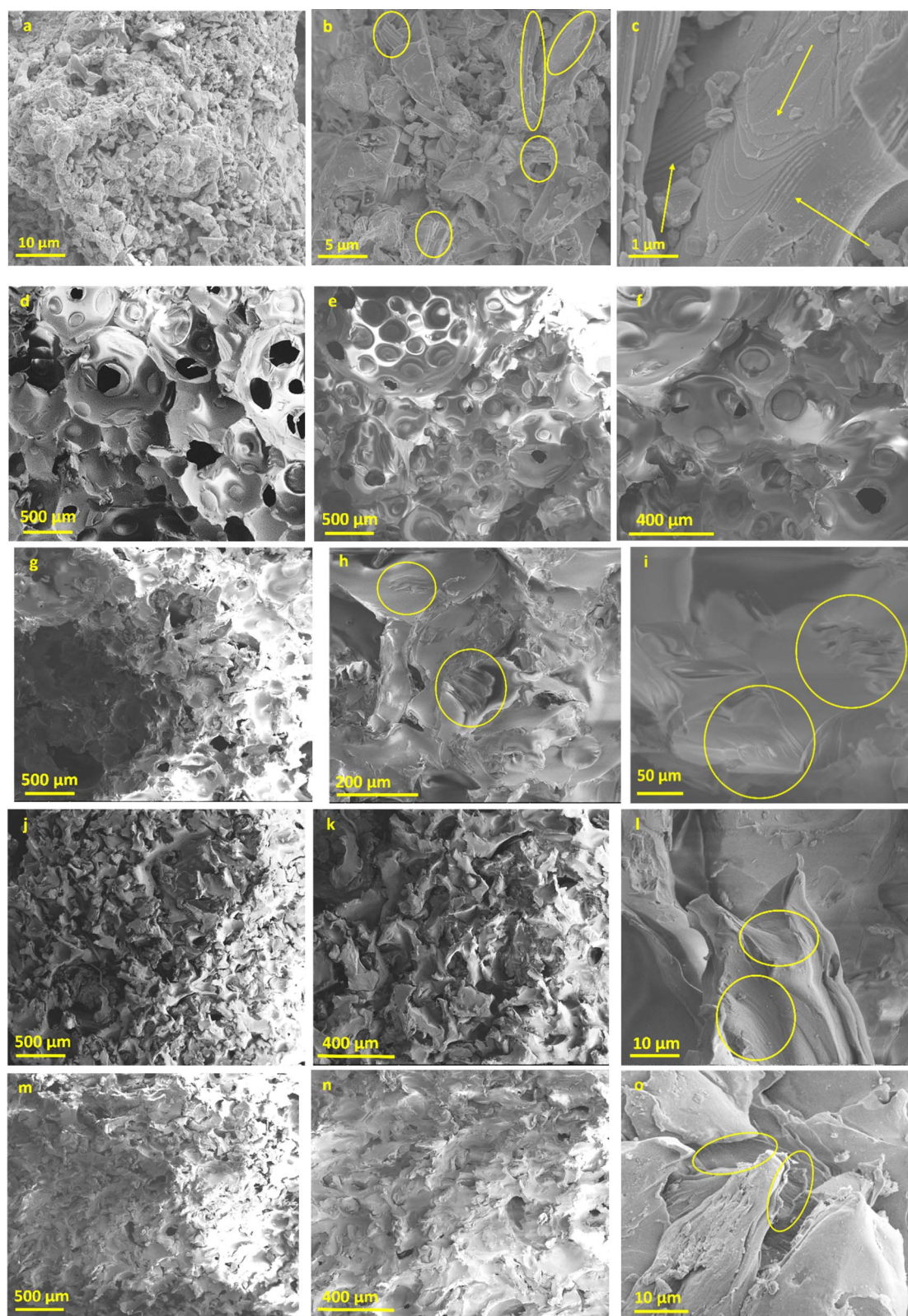Fig. 1 FT-IR analysis of the blank sample (black line) and MXenes-based polyurethane foams.

Fig. 2   SEM micrographs of Nb$_2$AlC-MXenes (a, b, and c), blank sample (sample 0) in different areas (d, e, and f), Sample A loaded with 0.3 g MXenes (g, h, and i), Sample B loaded with 0.5 g MXenes (j, k, and l), respectively Sample C loaded with 0.7 g MXenes (m, n, and o); the yellow arrows indicate detailed micrographs of the folded MXenes (image c), while the yellow circles evidenced the presence of exfoliated MXenes embedded in the walls of the PUR foams (detail images i, l, and o).
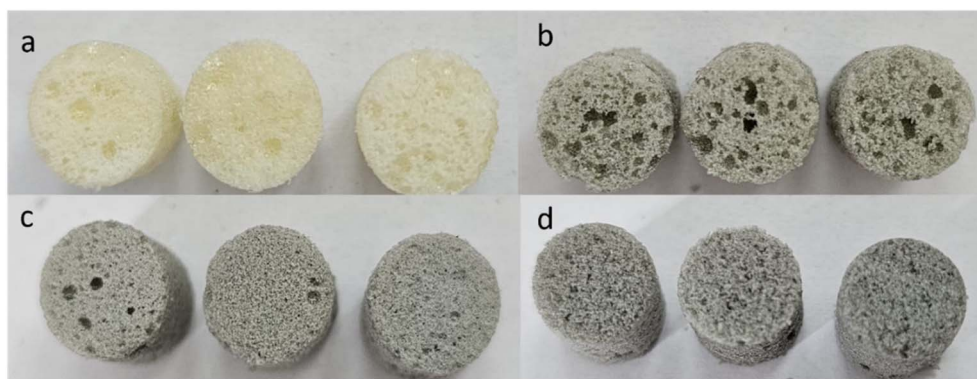
Fig. 3 Images of blank sample (Sample 0) (a), Sample A (b), Sample B (c), and Sample C (d) that present the uniform distribution of MXenes.

Nb_2AlC-MXenes appear irregular and powder-like at low magnifications (Fig. 2a, 1000×). However, at higher magnifications (Fig. 2b, 10 000×), certain areas (highlighted by yellow circles) reveal lamellar structures. In the detailed image taken at 50 000× magnification (Fig. 2c), the yellow arrows further illustrate these lamellar features, showing that the MXenes are compactly folded, these results being in good agreement with the literature data.[31,32]

For the PUR blank sample, analysis was conducted in different areas at two magnifications (Fig. 2d and e, 100×; Fig. 2f, 200×), indicating large pore formation. For Sample A, loaded with the lowest concentration of Nb_2AlC, Fig. 2g revealed a porous structure at 100× magnification. The detailed images (highlighted by yellow circles) further showed the presence of exfoliated Nb_2AlC (Fig. 2h and i). This suggests that dispersing **MXenes** into the polyol component followed by curing disrupted the naturally folded structure of the carbide-based MXenes. For the other two samples loaded with 0.5 g and 0.7 g MXenes, respectively, more compact structures were observed as the pore size decreased in Sample B (Fig. 2j and k) and Sample C (Fig. 2m and n). The detailed images for these samples (Fig. 2l and o) also showed exfoliated/detached MXenes embedded in the PUR matrix. Another important factor is the dispersibility of the MXenes within the PUR matrix, which leads to a uniform appearance of the samples and ensures an even distribution of the powder-like component throughout the polymer matrix, as illustrated in Fig. 3.

In the ESI,† we provide spectra for all samples and element distributions to support our SEM analysis, obtained *via* the EDX mapping procedure (Fig. S1–S4†). Two magnifications, at 200 μm and 10 μm, reveal consistent information about the presence of MXenes in all PET-based PUR foam-modified samples, confirmed by the uniform distribution of Al and Nb at both larger and smaller scales. For Sample 0, the EDX mapping and spectrum confirm the presence of C, N, and O, characteristic of the elemental composition of PUR (Fig. S1†). In PUR samples modified with varying Nb_2AlC concentrations, EDX mapping at smaller scales (10 μm) shows that the MXenes are covered by the polymer matrix, as indicated by the presence of N from the blank PUR sample. Element quantification for all samples (Fig. S1b, S2b, S3b, and S4b†) shows an increase in Al atomic

percentage from 0.19% to 0.36% as MXenes concentration rises from Sample A (Fig. S2-b†) to Sample C (Fig. S4-b†). However, for Sample C, the Nb element had lower atomic value compared to previous samples, which can be attributed to an agglomeration of the filling agent and probably poorer dispersion conditions in the polymer matrix (Fig. S4†).

To prove that the pore size is lower as the content of MXenes increased, the pore size distribution and the mean diameter of the pores for the blank sample and PUR foams loaded with Nb_2AlC were obtained from SEM images by measuring around 200 pores. Consequently, the pore sizes were found to range from 52 μm to 485 μm, 40 μm to 537 μm, 40 μm to 253 μm, and 35 μm to 208 μm for Sample 0, A, B, and C, respectively (Fig. 4). The histogram was best fitted with the Gauss function. The highest percentage of pores for Samples 0, A, B, and C were found to be within 74–182 μm, 54–171 μm, 83–170 μm and 58–173 μm diameter size range having the mean diameter 119 ± 67 μm (Sample 0), 145 ± 70 μm (Sample A), 131 ± 41 μm (Sample B), 80 ± 34 μm (Sample C). Thus, by increasing the concentration of MXenes in the polymer matrix, the mean diameter of the pores decreased as suggested by the areas investigated through SEM analysis.

### 3.4 Density of the PUR-MXenes-based composites

According to the determinations performed using ASTM D7710-14 as described in Section 2.3.4, the densities of the PUR foams varied from 120.51 ± 14.55 kg m^{-3} for Sample 0 to 128.75 ± 3.03 kg m^{-3} for Sample A, 148.82 ± 7.07 14.55 kg m^{-3} for Sample B, respectively 165.74 ± 25.05 kg m^{-3} for Sample C.

Fig. 5 presents the evolution of the density of the PUR specimens with the **MXenes** content. As expected, the density increases with the concentration of **MXenes** loaded and is in good agreement with the pore size distribution (densities increase, pore size decrease).[33,34]
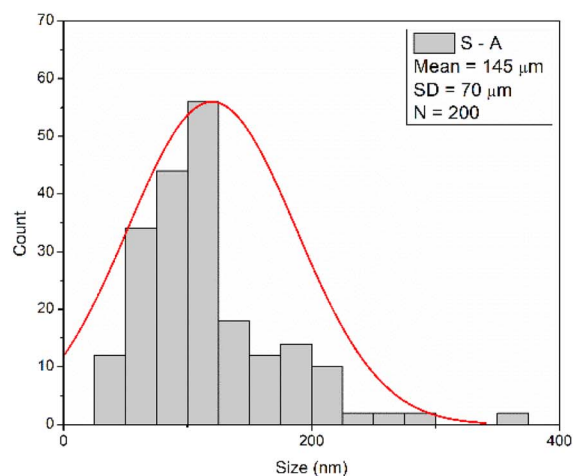
3.5 XRD characterization of the PUR-formulated foams

To prove the characteristic diffraction peaks of Nb_2AlC the next stage of this study consisted of performing XRD analysis on the MXenes powder and the PUR-based foams loaded with MXenes. Thus, the XRD pattern of the PUR blank sample, Sample
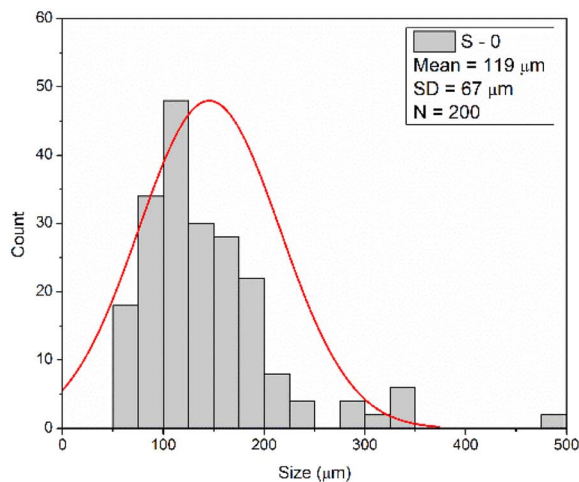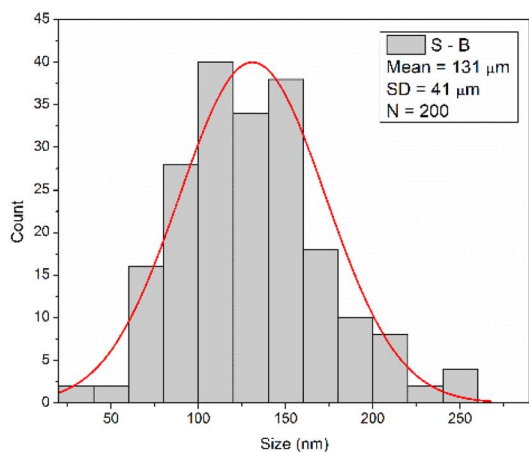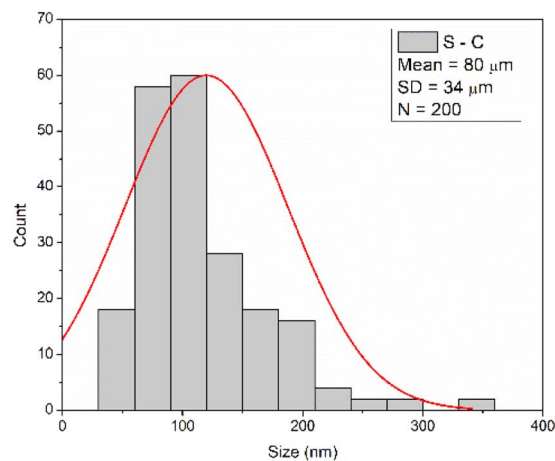
Fig. 4 Pore size distribution and mean size diameter for Sample 0 (a), Sample A (b), Sample B (c), and Sample C (d).

0 (Fig. 6 – black line), presents a broad diffraction peak at ~20°, which agrees with other XRD studies.[35]

The Nb$_2$AlC presents a set of diffraction peaks at $2\theta = 12.86$, 25.77, 33.32, 33.86, 35.11, 37.44, 38.84, 40.63, 42.42, 52.09, 57.64, 58.89, 59.61° which can be unambiguously ascribed to different (*hkl*) reflections of hexagonal Nb$_2$AlC with $a = b = 0.31$ nm; $c = 1.38$ nm, according to ICDD (International Centre for Diffraction Data) database, card no. 030-0033. Further, with increasing the Nb$_2$AlC concentration in the PUR matrix (*i.e.* from 0.3 g up to 0.7 g) it is obvious the formation of new diffraction peaks, which are given by (002), (100), (101), (102), (103), (106), (110) atomic planes of Nb$_2$AlC (Fig. 6a). The crystallinity of Nb$_2$AlC was evaluated by the Scherrer equation, which gives the relationship between the mean crystallite size

and the broadening of the diffraction peaks.[36] The analysis of the (103) main diffraction peak with a pseudo-Voigt fit reveals that the Full Width at Half Maximum (FWHM) is ~0.27 (Nb$_2$AlC), while for the composites its value ranges between ~0.47 and ~0.30 as the concentration increases. By applying the Scherrer equation, it was found that τ ~30 nm for the initial Nb$_2$AlC powder varies from ~15 nm to ~27 nm as the Nb$_2$AlC increases in the PUR matrix. At the same time, one can note a shift of the (103) diffraction peak at smaller values from $2\theta = 38.95°$ towards $2\theta = 38.69°$, which indicates a non-negligible tensile lattice strain in Nb$_2$AlC after embedding in the PUR matrix.

Likewise, Rietveld refinement of Sample C (Fig. 6b) indicates the co-existence of PUR and Nb$_2$AlC, and in addition, it shows
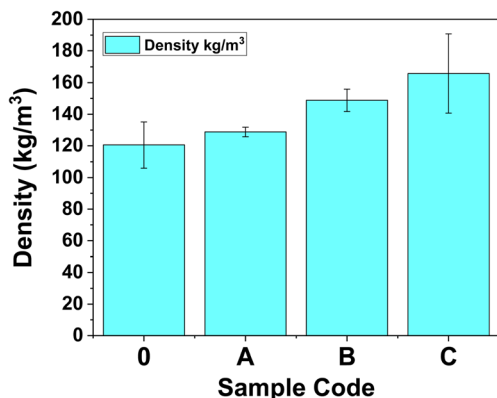
Fig. 5 Densities of the samples *versus* the MXenes content in the PUR foam specimens.

the presence of a non-negligible lattice strain, $\varepsilon \sim +0.16\%$. At the same time, the mean crystallite size derived from the Rietveld refinement ~ 28 nm is very close to the initial Nb_2AlC powder. Thus, the XRD results are in good agreement with the morphological aspect of the samples proved by the detailed SEM images (Fig. 2f, i, l, and o respectively) that indicated a less folded structure of the Nb_2AlC embedded in the PUR foam structure.

3.6 Compression tests of the polyurethane foams

Considering the practical application of the PUR-based samples filled with MXenes that can be used as insulator materials that can cover electronic equipment for EMI shielding compression tests were employed to determine the mechanical behavior of all specimens under loading.

Thus, Fig. 7 illustrates the stress–strain plots for compression tests, while Table 2 compares the maximum force measured for each specimen. The comparison of the mechanical performance of the PUR-based samples was made based on the mean value of force expressed in N (Table 2 – last column).

The compression mechanical tests of the foams confirmed that the compression stress and compression strain increased for the samples in which the highest concentration of reinforcing agent was added. Thus, the best mechanical performances were registered by Sample C, respectively Sample B. Thus, the next analysis will be performed for Sample 0 and C, comparatively.

Based on the allure of the curves it can be noticed that three regions characterize the mechanical behavior of all samples, namely the elastic zone, the plateau zone, and the densification zone which were confirmed also by Petrů and Novák.[37]

The first step of the compression test takes place from the moment the cell walls approach under continuous loading until they begin to collapse. In the plateau stage, buckling of the samples under pressure occurs, while in the final stage, cell wall collapse occurs until reaching the opposite walls, which determines the densification of polyurethane foam.

The presence of MXenes extended the elastic region and increased the slope of the curves due to the higher rigidity of the cellular walls. For the plateau region, the slope increased
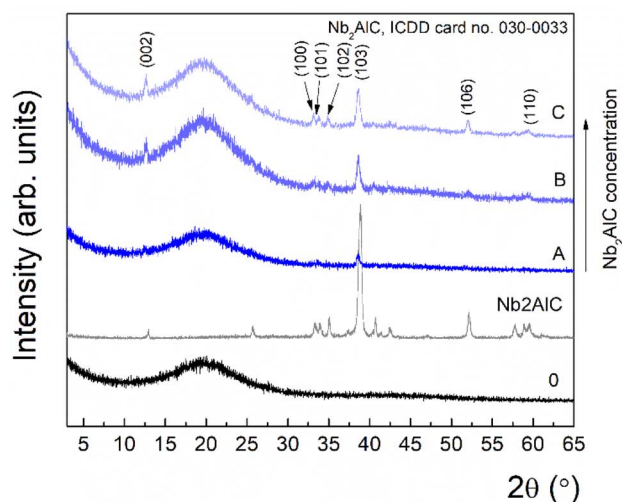
(a)
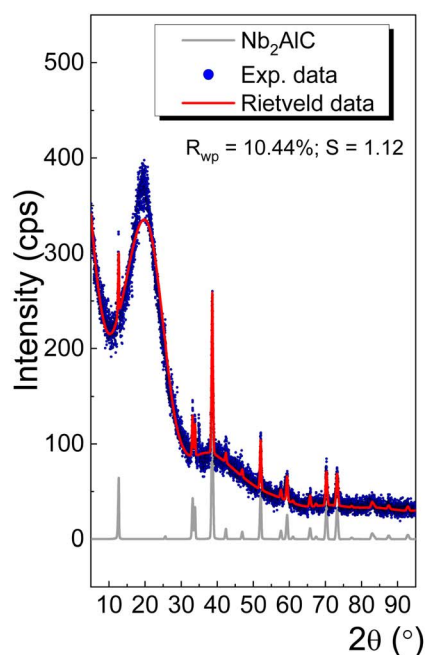
(b)

Fig. 6 The XRD pattern for Nb_2AlC and PUR loaded with Nb_2AlC (a), and Rietveld refinement for Sample C (b).

slightly due to the incorporation of the Nb_2AlC powder in the cellular structure. This led to a reinforcing of the cell walls that determined a higher mechanical resistance of the porous matrix.[38] Furthermore, the propagation of the crack seems to be delayed giving higher resistance to complete breaking/collapse. All these mechanical improvements were registered for all samples compared with the blank sample and are influenced by the highest concentration of the filling agent and the uniform distribution of the fillers in the structure of the foams. The
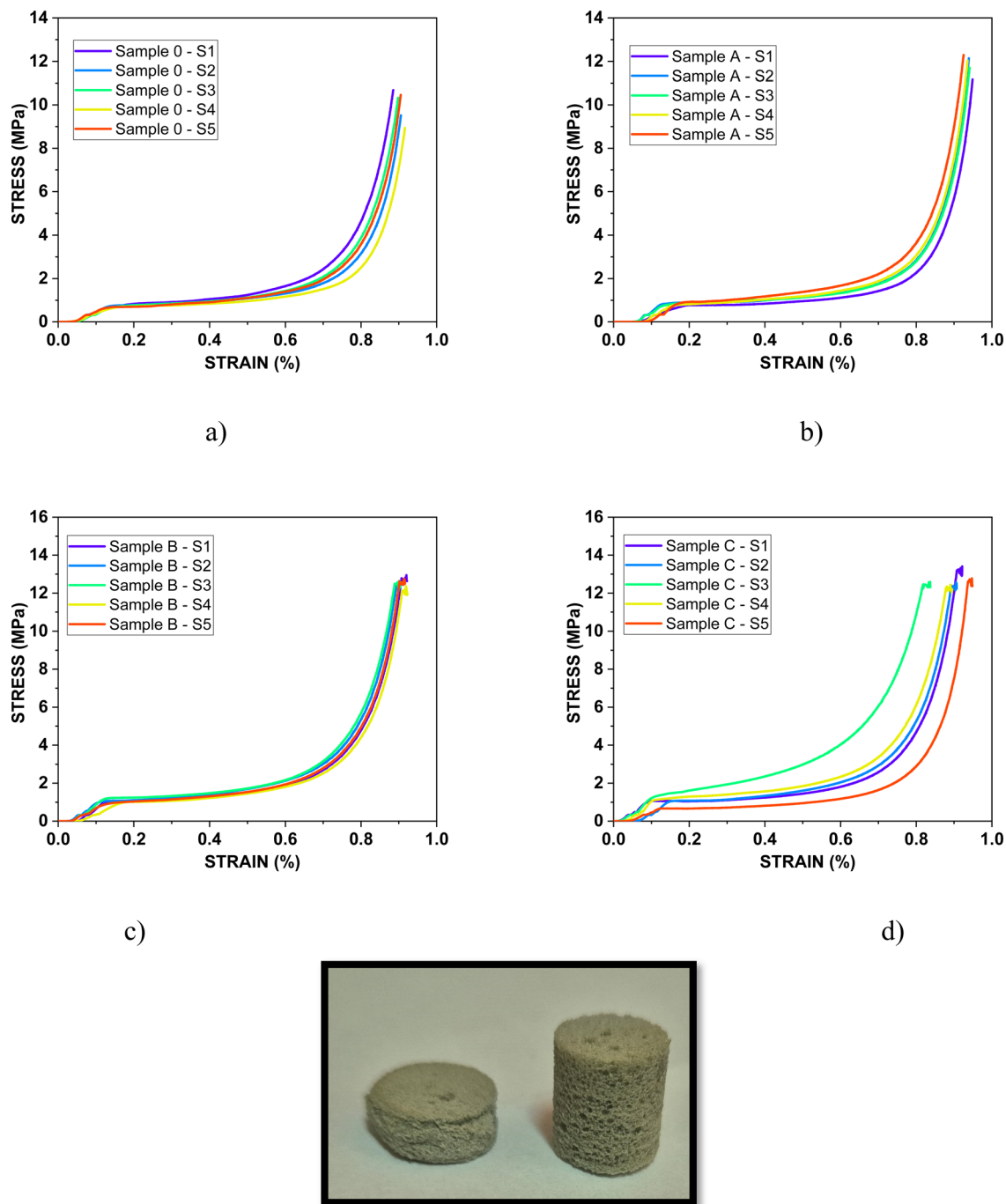
Fig. 7 Stress–strain plots for Samples 0, A, B, and C and the optical image of the sample recorded before and after the compression test.

Table 2 Maximal forces measured during compression tests

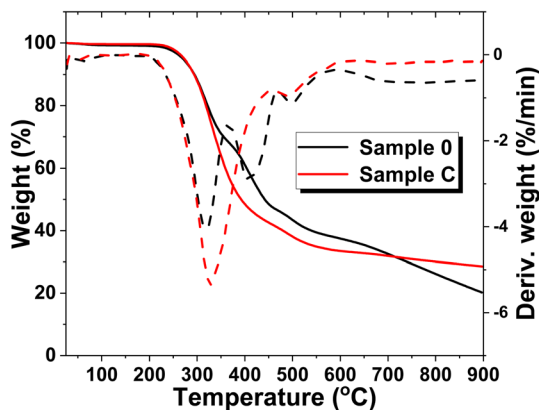| Sample code	Max force (N) Specimen 1	Max force (N) Specimen 2	Max force (N) Specimen 3	Max force (N) Specimen 4	Max force (N) Specimen 5	Mean value, (N)
Sample 0	881.58	737.24	869.04	716.41	846.43	810.14
A	930.64	982.45	984.87	992.75	974.95	973.13
B	1007.06	1012.88	1019.48	1012.76	1014.68	1013.37
C	1017.39	1016.96	1010.46	1010.73	1013.03	1013.71

Fig. 8 TGA and DTA analysis of blank sample, Sample 0, and polyurethane foams filled with the highest concentration of MXenes (0.7 g), Sample C.

values registered for the compressive stress indicate that these types of materials may be suitable for use in the civil engineering industry.[39–41]

3.7 Thermal characterizations of the polyurethane foams

To explore the potential applications of the formulated foams, additional insights can be gained through TGA and DSC analyses. Before 230 °C, all specimens exhibited a similar weight loss of approximately 5%, attributed to the evaporation of water and the removal of low molecular weight additives. In Fig. 8, two major decomposition stages are identified within the temperature ranges of 230–320 °C and 450–480 °C, respectively. These stages correspond to the characteristic two-step decomposition of urethane bonds and the cleavage of polymer chains[42] in Sample C (which contains the highest concentration of MXenes, Fig. 8 – red line). In contrast, Sample 0 (Fig. 8 – black line) shows three distinct stages of decomposition, with an additional step observed between 350–450 °C.

Between 320–400 °C, the Gram-Schmidt profile indicates the degradation of volatile compounds, the release of isocyanates and alcohols, and the breakdown of hard segments.[43] Beyond 500 °C, the polymer matrix is completely degraded in all

samples. Despite both samples experiencing significant weight loss between 230–500 °C, Sample C demonstrates higher thermal stability than Sample 0, as evidenced by a higher residual weight of approximately 30% compared to 20% for the blank sample. Additionally, the weight loss in Sample C occurs at a slower rate compared to Sample 0, suggesting an enhancement in thermal properties due to the presence of MXenes within the polyurethane foam structure. This improvement is further supported by the absence of the weight loss step observed in the blank sample, but not in Sample C.

Fig. 9 is composed of two main sections describing the DSC graph for the thermal behavior of Sample 0, respectively Sample C and a set of microscope images taken during the DSC analysis showing the differences in structural change at three different temperatures of both samples.

Sample 0 shows a slightly abrupt slope between 280 °C and 350 °C, indicating a more rapid exothermic reaction, likely due to the breakdown of the PUR matrix without MXenes compared with Sample C. However, comparing the T_g of the two samples, it can be noticed that the values are close, the difference being around 10 °C. Taking into account that Sample C has a lower T_g, it can be concluded that the foam is more flexible compared to Sample 0 (compression tests proved an extension of the elastic zone) and the macromolecular chains slide over each other more easily, due to the presence of detached/exfoliated MXenes (evidenced by SEM and XRD analysis).

3.8 EMI shielding properties

To evaluate the EMI shielding properties for the synthesized materials at microwave frequencies, we employed a waveguide-based experimental setup[25] to analyse their reflection and transmission properties covering frequencies from 8.2 to 12.4 GHz, known as the X band. This frequency range is particularly important for high-frequency applications being extensively used in radar systems for air control, weather, terrestrial and space communications, traffic light motion sensors, and RF sources for particle accelerators in medical applications. EMI poses significant issues by severely degrading the performance of electronics affecting not only their life expectancy but also altering the quality signal of the device. To mitigate these
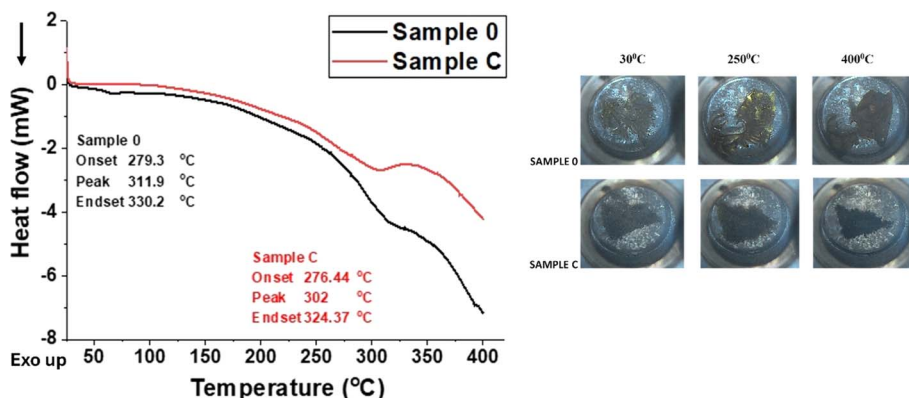

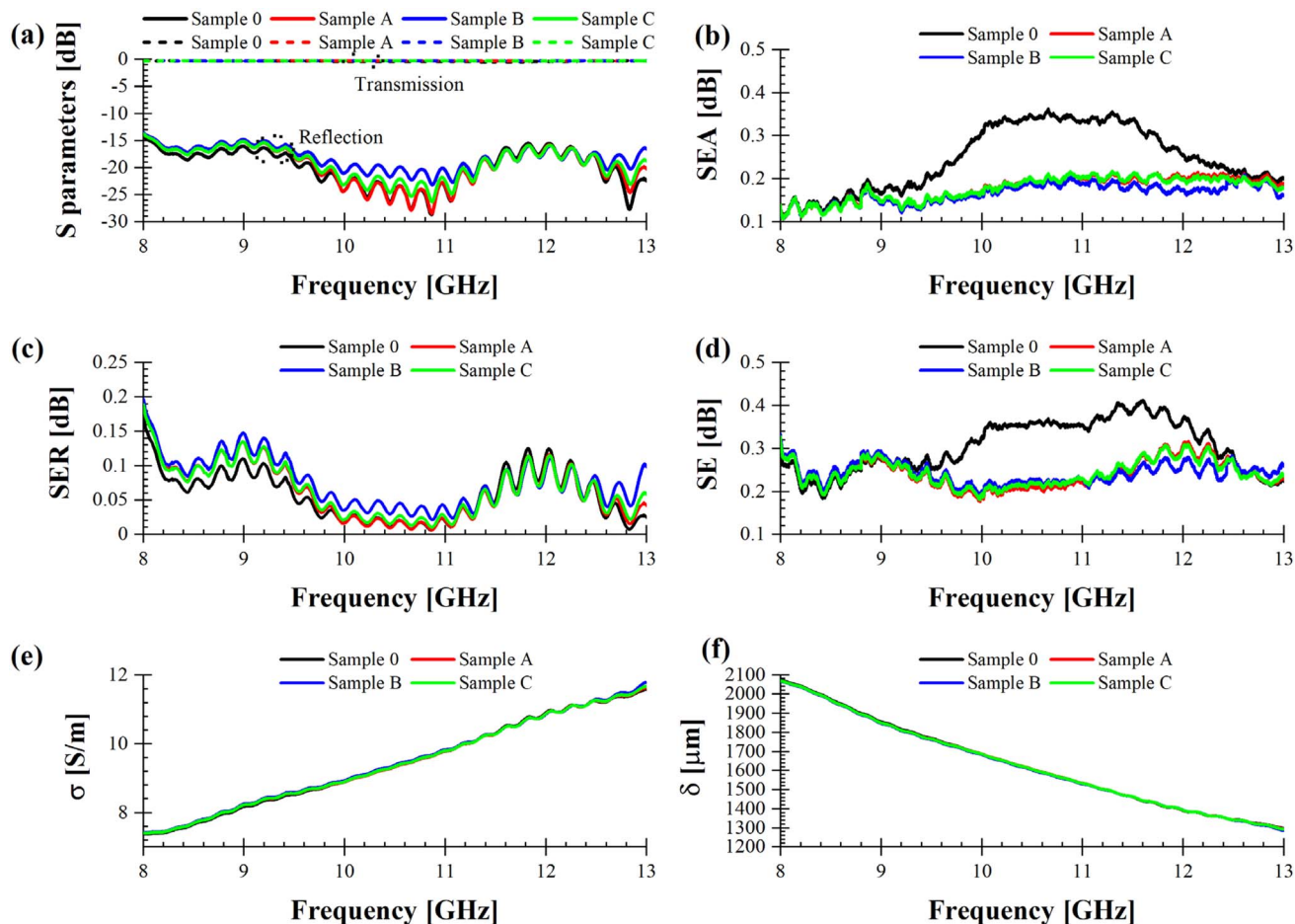Fig. 9 DSC and optical microscopy for the samples at different temperatures.

Fig. 10 (a) Measured S parameters. Extracted (b) SE_A, (c) SE_R, (d) SE, (e) conductivity, and (f) skin depth for blank PUR foam and the specimens loaded with MXenes in the X band.

issues, various materials have been investigated for EMI protection, including pristine conductive polymers or hybrid composites of the polymers with carbonaceous materials like graphene, carbon nanotubes, and other nanofillers.[44] Over the past decade, the development of two-dimensional (2D) atomically thin structures has led to new materials with EMI shielding capabilities comparable to carbon-based nanomaterials, such as MXenes which is a new class of transition metal carbides, nitrides, and carbonitrides.[45] Therefore, materials can be engineered to provide either EM transparency or EMI shielding properties based on specific application needs.[26]

As previously described in Section 2.3.9, the EMI shielding capabilities of Sample 0, A, B, and C, were determined using a calibrated VNA connected to two X-band waveguide transitions. The specimens were placed between these transitions, allowing us to record the scattering (S) parameters at the two ports of the VNA. Based on the measured S parameters (Fig. 10a), all relevant quantities were calculated using eqn (1)–(4) as outlined in Section 2.3.9.

Fig. 10b–d show that Sample 0 (solid black line) provides the best performance between 9 and 13 GHz, mostly due to a bigger high-frequency absorption in the upper part of the X band; this means that the addition of MXenes does not entail a monotonic

change of sample's performance in terms of EMI shielding in this particular frequency range. This could be ascribed in principle to an agglomeration of the filling agent in the polymeric matrix. However, we can observe an improvement of the EMI shielding characteristics in the 8–9 GHz frequency range (Fig. 11), which could be suitable for dedicated military and/or civilian applications requiring specific frequencies for secured telecommunications.

Even if all the characterized samples exhibit good transmission and reflection properties ($|S_{21}|$ is always between 0 and −0.5 dB, whereas $|S_{11}|$ is always between −15 and −30 dB), Fig. 11 demonstrates that Sample B (solid blue line) offers the best EMI shielding performance (Fig. 11d) mostly due to the highest SE_R values (Fig. 11c), which translate into a bigger attenuation of the EM signal propagating in the waveguide, *i.e.*, a degradation of the reflection coefficient with about 1.5 dB with respect to Sample 0. This result is corroborated by Fig. 11e, in which the conductivity σ of Sample B spans in the range 7.4–8.2 S m^{-1}. This value is at least 50% greater than the conductivity of seawater, which is about 5 S m^{-1}. Hence, the enhancement of the conductivity comes from the concentration of MXenes. Finally, the values of the skin depth δ (Fig. 11f) are strictly related to those of the conductivity, for the following reason: an
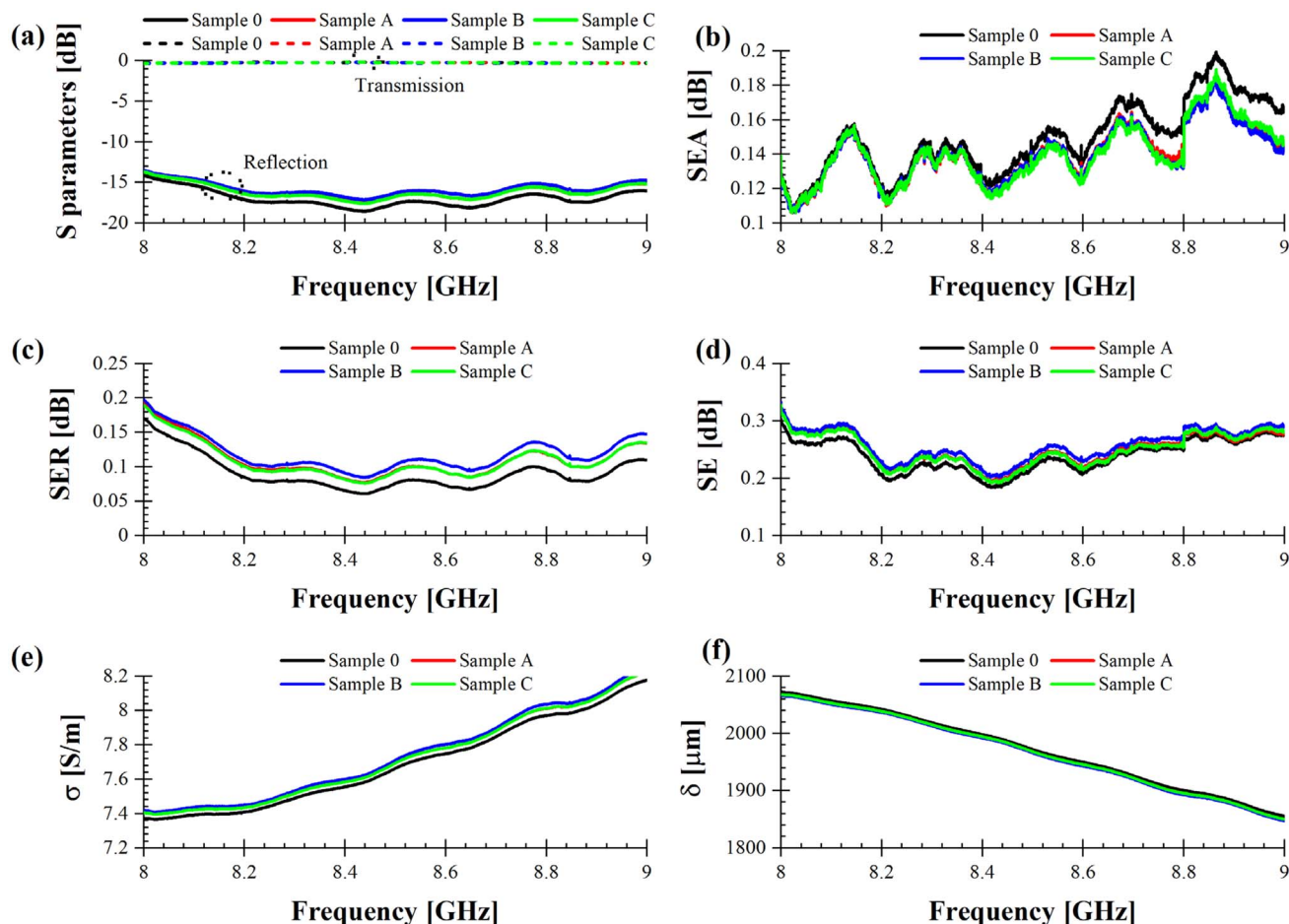
Fig. 11 (a) Measured S parameters. Extracted (b) SE_A, (c) SE_R, (d) SE, (e) conductivity, and (f) skin depth for blank PUR foam and the specimens loaded with MXenes in the 8–9 GHz band.

increase of σ entails a decrease of δ and, most of all, a general rule of thumb for any conductive material is to have a thickness which is at least double with respect to its skin depth, to prevent the penetration of the high-frequency EM field inside the materials itself and, hence, additional losses. Since the thickness of all specimens' spans between 5.1 mm (Sample C), 5.82 mm (Sample B), 5.51 mm (Sample A) and 6.61 mm (Sample 0) it is evident that the skin depth has an abrupt decrease for increasing frequencies since the thickness of each sample becomes much greater than the corresponding skin depth.

As a whole, Sample B has the potential to be a good EMI shielding material and we expect that a further increase of the MXenes content will enhance the shielding properties, by keeping at the same time an acceptable degree of mechanical flexibility. The latter characteristic is an added value since it can follow the shape of the object to shield it from EMI. We stress here that for all the composite materials described in this work, the results are consistent and reproducible after systematic measurements.

4 Conclusions

This study highlighted the synthesis and characterization of polyurethane foams manufactured from industrial PET wastes and MXenes. Thus, the polyol component was comprised not only of different commercial polyols but also of glycolysis products resulting from PET depolymerization in the presence of DEG bringing added value to the newly formulated products in terms of recycling plastic wastes. The resulting PUR foam specimens were characterized by FT-IR, SEM, density measurements, XRD, mechanical, and thermal analysis, as well as EMI shielding capabilities.

The FT-IR results showed the presence of urethane bond formation in all cases. SEM micrographs revealed that as the MXenes content increased from Sample A to Sample C, the structure became more compact, with a statistically significant reduction in pore size diameter. Additionally, SEM images showed a detached or unfolded appearance of the close-packed lamellar structures of Nb_2AlC within the polymer matrix. EDX analysis and mapping indicated the presence and incorporation of Mxenes in all PUR samples both at larger (200 microns) and smaller scales (10 microns). The density of the PUR foams increased from 120 to nearly 170 kg m^{-3} with higher MXenes content. XRD analysis demonstrated tensile lattice strains in Nb_2AlC after incorporation into the PUR matrix, indicated by a shift in the (103) diffraction peak from $2\theta = 38.95°$ to $2\theta = 38.69°$ proving a less folded structure compared with the packed

lamellar structure of the pristine Mxenes. Compression tests revealed that Sample B and Sample C had similar performance, while the thermal behavior of Sample C was not significantly different from that of Sample 0.

Regarding EMI shielding properties, Sample B has the potential to become an effective EMI shielding material in the 8–9 GHz band, which could be suitable for dedicated military and/or civilian applications requiring specific frequencies for secured telecommunications.

It is anticipated that increasing the MXenes content further will enhance the shielding effectiveness while keeping an acceptable degree of mechanical performance.

Data availability

Data supporting this study are openly available from the corresponding authors.

Conflicts of interest

All authors declare no conflicts of interest.

Acknowledgements

References

1 T. Muringayil Joseph, S. Azat, Z. Ahmadi, O. Moini Jazani, A. Esmaeili, E. Kianfar, J. Haponiuk and S. Thomas, Polyethylene terephthalate (PET) recycling: A review, *Case Stud. Chem. Environ. Eng.*, 2024, **9**, 100673.

2 P. Sarda, J. C. Hanan, J. G. Lawrence and M. Allahkarami, Sustainability performance of polyethylene terephthalate, clarifying challenges and opportunities, *J. Polym. Sci.*, 2022, **60**(1), 7–31.

3 M. G. Kibria, N. I. Masuk, R. Safayet, H. Q. Nguyen and M. Mourshed, Plastic Waste: Challenges and Opportunities to Mitigate Pollution and Effective Management, *Int. J. Environ. Res.*, 2023, **17**(1), 20.

4 F. Zhang, F. Wang, X. Wei, Y. Yang, S. Xu, D. Deng and Y.-Z. Wang, From trash to treasure: Chemical recycling and upcycling of commodity plastic waste to fuels, high-valued chemicals and advanced materials, *J. Energy Chem.*, 2022, **69**, 369–388.

5 J. Yang, Z. Li, Q. Xu, W. Liu, S. Gao, P. Qin, Z. Chen and A. Wang, Towards carbon neutrality: Sustainable recycling and upcycling strategies and mechanisms for polyethylene terephthalate *via* biotic/abiotic pathways, *Eco-Environ. Health*, 2024, **3**(2), 117–130.

6 R. Meys, F. Frick, S. Westhues, A. Sternberg, J. Klankermayer and A. Bardow, Towards a circular economy for plastic packaging wastes – the environmental potential of chemical recycling, *Resour., Conserv. Recycl.*, 2020, **162**, 105010.

7 F. Weiland, M. Kohlstedt and C. Wittmann, Biobased *de novo* synthesis, upcycling, and recycling—the heartbeat toward a green and sustainable polyethylene terephthalate industry, *Curr. Opin. Biotechnol.*, 2024, **86**, 103079.

8 A. Bohre, P. R. Jadhao, K. Tripathi, K. K. Pant, B. Likozar and B. Saha, Chemical Recycling Processes of Waste Polyethylene Terephthalate Using Solid Catalysts, *ChemSusChem*, 2023, **16**(14), e202300142.

9 E. Rusen, A. Mocanu, F. Rizea, A. Diacon, I. Calinescu, L. Mititeanu, D. Dumitrescu and A. M. Popa, Poly(ethylene terephthalate) Recycled from Post-Consumer Soft-Drinks Bottles I.Poly(ethylene terephthalate) depolymerization by glycolysis process, *Mater. Plast.*, 2013, **50**(2), 130–133.

10 E. Rusen, A. Mocanu, F. Rizea, A. Diacon, I. Calinescu, L. Mititeanu, D. Dumitrescu and A. M. Popa, Post-consumer PET Bottles Recycling II. PET depolymerization using microwaves, *Mater. Plast.*, 2013, **50**(3), 201–207.

11 E. Rusen, A. Mocanu, D. Fiat, A. M. Dumitrescu, P. O. Stanescu and A. Diacon, Straightforward Manufacturing of Polyurethane Adhesives and Foams from Post-consumer Poly(ethylene terephthalate) (PET) Bottles, *Mater. Plast.*, 2015, **52**(2), 209–213.

12 A. C. Mârțolea, A. Mocanu, P. O. Stănescu, O. Brincoveanu, C. Orbeci, R. Irodia, C. Pîrvu, A. Dinescu, C. Bobirica and E. Rusen, Synthesis and characterization of polyurethane flexible foams provided from PET derivatives, fly ash, and glass wastes, *Heliyon*, 2023, **9**(12), e23097.

13 A. C. Mârțolea, C. Orbeci, E. Rusen, P. O. Stanescu, O. Brincoveanu, R. Irodia, C. Pîrvu, A. Dinescu, C. Bobirica and A. Mocanu, Design of polyurethane composites obtained from industrial plastic wastes, pyrite and red mud, *Constr. Build. Mater.*, 2023, **405**, 133319.

14 R. M. Ronchi, J. T. Arantes and S. F. Santos, Synthesis, structure, properties and applications of MXenes: Current status and perspectives, *Ceram. Int.*, 2019, **45**(15), 18167–18188.

15 M. Naguib, V. N. Mochalin, M. W. Barsoum and Y. Gogotsi, 25th Anniversary Article: MXenes: A New Family of Two-Dimensional Materials, *Adv. Mater.*, 2014, **26**(7), 992–1005.

16 M. Naguib, M. Kurtoglu, V. Presser, J. Lu, J. Niu, M. Heon, L. Hultman, Y. Gogotsi and M. W. Barsoum, Two-Dimensional Nanocrystals Produced by Exfoliation of Ti3AlC2, *Adv. Mater.*, 2011, **23**(37), 4248–4253.

17 Z. Li, Y. Sun, B. Zhou, Y. Feng, C. Liu and C. Shen, Flexible thermoplastic polyurethane/MXene foams for compressible electromagnetic interference shielding, *Mater. Today Phys.*, 2023, **32**, 101017.

18 E. G. Kıvrak, K. K. Yurt, A. A. Kaplan, I. Alkan and G. Altun, Effects of electromagnetic fields exposure on the antioxidant defense system, *J. Microsc. Ultrastruct.*, 2017, **5**(4), 167–176.

19 R. Verma, P. Thakur, A. Chauhan, R. Jasrotia and A. Thakur, A review on MXene and its' composites for electromagnetic interference (EMI) shielding applications, *Carbon*, 2023, **208**, 170–190.

20 A. Iqbal, J. Kwon, M. K. Kim and C. M. Koo, MXenes for electromagnetic interference shielding: Experimental and theoretical perspectives, *Mater. Today Adv.*, 2021, **9**, 100124.

21 L. Liang, C. Yao, X. Yan, Y. Feng, X. Hao, B. Zhou, Y. Wang, J. Ma, C. Liu and C. Shen, High-efficiency electromagnetic interference shielding capability of magnetic Ti3C2Tx MXene/CNT composite film, *J. Mater. Chem. A*, 2021, **9**(43), 24560–24570.

22 Y. Liu, Y. Liu and X. Zhao, MXene Composite Electromagnetic Shielding Materials: The Latest Research Status, *ACS Appl. Mater. Interfaces*, 2024, **16**(31), 41596–41615.

23 H. Zhang, J. Wan, R. Wu, Y. Chen, H. Yu and S. Shi, MXenes for electromagnetic interference shielding: Insights from structural design, *Carbon*, 2024, **218**, 118716.

24 K. Chand, X. Zhang and Y. Chen, Recent progress in MXene and graphene based nanocomposites for microwave absorption and electromagnetic interference shielding, *Arabian J. Chem.*, 2022, **15**(10), 104143.

25 E. Rusen, A. Mocanu, O. Brincoveanu, A. Boldeiu, C. Romanitan, M. Aldrigo, S. Iordănescu, A. Diacon, G. Toader and R. Gavrila, MXenes and polymeric colloids nanocomposites for EMI shielding, *J. Mater. Chem. C*, 2024, **12**(30), 11586–11593.

26 Y. Tan, H. Luo, H. Zhang, X. Zhou and S. Peng, Lightweight graphene nanoplatelet/boron carbide composite with high EMI shielding effectiveness, *AIP Adv.*, 2016, **6**(3), 035208.

27 M. H. Al-Saleh and U. Sundararaj, Electromagnetic interference shielding mechanisms of CNT/polymer composites, *Carbon*, 2009, **47**(7), 1738–1746.

28 P. S. Lee, S.-C. Kim, E. T. Tikue and S. M. Jung, One-Pot Reaction of Waste PET to Flame Retardant Polyurethane Foam, *via* Deep Eutectic Solvents-Based Conversion Technology, *J. Polym. Environ.*, 2022, **30**(1), 333–343.

29 D. Cevher and S. Sürdem, Polyurethane adhesive based on polyol monomers BHET and BHETA depolymerised from PET waste, *Int. J. Adhes. Adhes.*, 2021, **105**, 102799.

30 T. Yousaf, A. Areeb, M. Murtaza, A. Munir, Y. Khan and A. Waseem, Silane-Grafted MXene (Ti3C2TX) Membranes for Enhanced Water Purification Performance, *ACS Omega*, 2022, **7**(23), 19502–19512.

31 S. Tu, F. Ming, J. Zhang, X. Zhang and H. N. Alshareef, MXene-Derived Ferroelectric Crystals, *Adv. Mater.*, 2019, **31**(14), 1806860.

32 P. A. Rasheed, R. P. Pandey, F. Banat and S. W. Hasan, Recent advances in niobium MXenes: Synthesis, properties, and emerging applications, *Matter*, 2022, **5**(2), 546–572.

33 M. Ghorbandoust, M. Fasihi and R. Norouzbeigi, Tuning pore size and density of rigid polylactic acid foams through thermally induced phase separation and optimization using response surface methodology, *Sci. Rep.*, 2024, **14**(1), 12395.

34 O. Gotkiewicz, M. Kirpluks, Z. Walterová, O. Kočková, S. Abbrent, P. Parcheta-Szwindowska, U. Cabulis and H. Beneš, Biobased Ultralow-Density Polyurethane Foams with Enhanced Recyclability, *ACS Sustain. Chem. Eng.*, 2024, **12**(4), 1605–1615.

35 B. Noureddine, S. Zitouni, B. Achraf, C. Houssém, D.-R. Jannick and G. Jean-François, Development and Characterization of Tailored Polyurethane Foams for Shock Absorption, *Appl. Sci.*, 2022, **12**(4), 2206.

36 A. L. Patterson, The Scherrer Formula for X-Ray Particle Size Determination, *Phys. Rev.*, 1939, **56**(10), 978–982.

37 M. Petrů and O. Novák, Measurement and Numerical Modeling of Mechanical Properties of Polyurethane Foams, *Aspects of Polyurethanes*, IntechOpen, 2017.

38 M. H. Moghim, M. Keshavarz and S. M. Zebarjad, Effect of SiO2 nanoparticles on compression behavior of flexible polyurethane foam, *Polym. Bull.*, 2019, **76**(1), 227–239.

39 V. Calderón, S. Gutiérrez-González, J. Gadea, Á. Rodríguez and C. Junco, 10 – Construction Applications of Polyurethane Foam Wastes, in *Recycling of Polyurethane Foams*, ed. S. Thomas, A. V. Rane, K. Kanny, V. K. Abitha and M. G. Thomas, William Andrew Publishing, 2018, pp. 115–125.

40 D. M. Constantinescu and D. A. Apostol, Performance and Efficiency of Polyurethane Foams under the Influence of Temperature and Strain Rate Variation, *J. Mater. Eng. Perform.*, 2020, **29**(5), 3016–3029.

41 K. B. Park, H. T. Kim, N. Y. Her and J. M. Lee, Variation of Mechanical Characteristics of Polyurethane Foam: Effect of Test Method, *Materials*, 2019, **12**(17), 2672.

42 R. Gu and M. M. Sain, Effects of Wood Fiber and Microclay on the Performance of Soy Based Polyurethane Foams, *J. Polym. Environ.*, 2013, **21**(1), 30–38.

43 J. Pagacz, E. Hebda, B. Janowski, D. Sternik, M. Jancia and K. Pielichowski, Thermal decomposition studies on polyurethane elastomers reinforced with polyhedral silsesquioxanes by evolved gas analysis, *Polym. Degrad. Stab.*, 2018, **149**, 129–142.

44 S. Parveen and A. Manju, Microwave Absorption and EMI Shielding Behavior of Nanocomposites Based on Intrinsically Conducting Polymers, Graphene and Carbon Nanotubes, in *New Polymers for Special Applications*, ed. Ailton De Souza, G., IntechOpen, Rijeka, 2012, ch. 3.

45 F. Shahzad, M. Alhabeb, C. B. Hatter, B. Anasori, S. Man Hong, C. M. Koo and Y. Gogotsi, Electromagnetic interference shielding with 2D transition metal carbides (MXenes), *Science*, 2016, **353**(6304), 1137–1140.